Journal of Water Process Engineering 71 (2025) 107200

Contents lists available at ScienceDirect

Journal of Water Process Engineering

journal homepage: www.elsevier.com/locate/jwpe

Neodymium removal and recovery from simulated NdFeB leachate using manganese ferrite nanoparticles

Joana Sousa [a], Daniela S. Tavares [a,b], João Pinto [a,*], Bruno Henriques [a], João Rocha [c], Tito Trindade [c], Nuno Lapa [d], Eduarda Pereira [a,b]

[a] Department of Chemistry, LAQV-REQUIMTE – Associated Laboratory for Green Chemistry, University of Aveiro, 3810-193 Aveiro, Portugal
[b] LCA – Central Laboratory of Analysis, University of Aveiro, 3810-193 Aveiro, Portugal
[c] Department of Chemistry, CICECO – Aveiro Institute of Materials, University of Aveiro, 3810-193 Aveiro, Portugal
[d] Department of Chemistry, LAQV-REQUIMTE, NOVA School of Science and Technology, NOVA University Lisbon, 2829-516 Caparica, Portugal

ARTICLE INFO

Editor: Ludovic F. Dumée

Keywords:
Rare earth elements
Neodymium
Ferrite
Magnets
Sorption
Response surface methodology

ABSTRACT

This study explores the use of manganese ferrite nanoparticles ($MnFe_2O_4$) for the removal and recovery of neodymium (Nd) from aqueous solutions, focusing on their potential application in wastewater treatment and environmental remediation. Neodymium, a critical element for the high-technology and energy industries, is increasingly present in aquatic environments due to its widespread use in devices such as computers, electric vehicles, and wind turbines. Through a series of kinetic, equilibrium, and desorption tests, the study optimized key operational parameters using Response Surface Methodology. Equilibrium analyses revealed that the Nd removal at equilibrium (q_e) reached 8 mg/g, while the maximum sorption capacity (q_m) was determined to be 9.2 mg/g. The results demonstrated a high removal efficiency (up to 90 %) under optimal conditions, which included a nanoparticle dose of 1000 mg/L, an initial neodymium concentration of 20 μmol/L, pH 6, and no salinity. The material showed great potential for neodymium recovery from synthetic magnet solutions, with removal rates exceeding 70 %. Desorption tests confirmed complete recyclability of the sorbent. These findings highlight manganese ferrite nanoparticles as a promising and sustainable approach for neodymium recovery.

1. Introduction

The rare earth elements (REEs), as defined by the International Union of Pure and Applied Chemistry (IUPAC), consis of 17 chemical elements, including the lanthanide series, along with yttrium and scandium. These elements possess very similar physical and chemical properties and are essential to the transition toward a green, low-carbon economy [1,2]. Their unique properties make them essential in the production of batteries for hybrid and electric cars, permanent magnets in hard drives and wind turbines, and various electronic devices and industrial catalysts [1,3,5–7]. Due to increasing demand, supply risks, and their importance in the development of new technologies, the European Commission [8] has classified several elements, including REEs, as "Critical Raw Materials". The U.S. Department of Energy, in its 2023 *Critical Materials Strategy* report [12], identified dysprosium, neodymium, praseodymium, and terbium as the most critical REEs by 2035. Neodymium (Nd) is particularly crucial, as it is extensively used in green energy production and strategic technologies [13], especially in NdFeB-based permanent magnets, which are the strongest available on the market, with magnetic strength 4 to 10 times greater than that of regular magnets [14,15].

NdFeB magnets are renowned for their superior magnetic properties, primarily consisting of the $Nd_2Fe_{14}B$ matrix phase [11]. They typically contain 25–30 % Nd, 60–70 % Fe, and around 1 % B (mass basis). However, depending on the application, additional elements like Pr, Dy, Tb, Co, Gd, Cu, Al, Ga, and Nb, among others, are added to enhance the efficiency of the magnet. These magnets have life cycles ranging from 2 to 3 years in consumer electronics to 20 to 30 years in wind turbines. Increasing demand for renewable energy and advanced technologies, transitions to clean energies, particularly in electric vehicles and wind power, are expected to increase demand by 8.6 % per year from 2022 to 2035 [11].

The potential for ecosystem disruption, combined with the fragility of the supply chain, highlights the importance of recovering Nd from secondary sources and reusing it in industrial applications. Leachates from the NdFeB permanent magnet industry, for example, have shown

* Corresponding author.
E-mail address: joao.pedro.pinto@ua.pt (J. Pinto).

https://doi.org/10.1016/j.jwpe.2025.107200
Received 16 December 2024; Received in revised form 17 January 2025; Accepted 5 February 2025
Available online 16 February 2025

promise as a viable source of neodymium, as demonstrated by studies like Brewer et al. [17] and Brião et al. [18]. Traditional methods for REEs' removal from waste typically involve pyrometallurgical and hydrometallurgical processes. Pyrometallurgy has several limitations, including the generation of slag and the loss of valuable metals. In contrast, hydrometallurgy uses aqueous reactions, including chemical precipitation, membrane separation, and ion exchange, which are easier to control and poses fewer environmental risks. Despite this, the extensive use of aggressive chemicals in hydrometallurgical is still not ideal in the prospect of a sustainable recovery of REEs such as Nd [6,13,15,19]. To reduce the environmental impacts associated with REEs recovery, sorption has emerged as a promising alternative for extracting REEs from aqueous environments [3,4,7,13]. This method minimizes the use of chemical reagents, works across a wide concentration range, and is generally regarded as environmentally friendly [15]. Additional advantages include high removal efficiency, ease of operation, low maintenance costs, and the ability to regenerate sorbents [19,20]. However, several factors should be considered when applying sorption as a REEs recovery technology, including the concentration of the element, sorbent dose, contact time, pH, temperature, and salinity/ionic strength. Beyond maximum sorption capacity, other factors influence the suitability of a sorbent, particularly its desorption and reuse potential. Desorption involves releasing substances from a solid surface into an acidic or basic solution, complementing sorption by enabling both high recovery efficiency and enhanced sorption performance. These factors are crucial in determining the overall effectiveness and sustainability of the sorbent in repeated cycles of use.

Ferrites have been proven effective as sorbents in water decontamination, removing toxic elements like mercury [23], arsenic [24,25], lead [26,27], and cadmium [28]. Spinel ferrites, a class of magnetic nanoparticles with the chemical formula MFe_2O_4 (where M represents transition metals like Fe, Cd, Ni, Co, Mn, Zn, Cu, and Mg) are particularly notable among these materials. In addition to their magnetic properties, they materials are valued for their low (eco)toxicity and cost-effectiveness [29,30]. Particularly, manganese ferrite nanoparticles ($MnFe_2O_4$) have shown effectiveness in removing REEs (La and Ce) and other critical elements (Cd, Pb, As, and Zn) from aqueous solutions. For example, Ghobadi et al. [7] demonstrated that modified $MnFe_2O_4$ nanoparticles exhibit a high sorption capacity, reaching 1001 mg/g for La^{3+} and 982 mg/g for Ce^{3+}, with optimal performance at a pH of 7 and an initial concentration of 500 mg/L. Under the same conditions, the unmodified $MnFe_2O_4$ nanoparticles displayed lower sorption capacities, with 785 mg/g for La^{3+} and 770 mg/g for Ce^{3+}. Similarly, Liu et al. [31] reported maximum sorption capacities of 1030 mg/g for La^{3+} and 1020 mg/g for Ce^{3+} (99.3 % removal) with modified nanoparticles, compared to 757 mg/g for La^{3+} and 751 mg/g for Ce^{3+} (76.2 % removal) with unmodified ones. These results consistently demonstrate that modified $MnFe_2O_4$ nanoparticles outperform their unmodified counterparts in sorption capacity. However, despite the enhanced performance of the modified nanoparticles, their modification incurs in higher costs. Therefore, it is essential to explore more sustainable processes that use unmodified nanoparticles, balancing efficiency with economic and environmental considerations. Recent studies also utilised $MnFe_2O_4$ nanoparticles for REEs removal from both single-element solutions [22] and complex mixtures [32].

Given the increasing demand for Nd in advanced technologies, coupled with the environmental and health risks associated to its contamination and toxicity, this study aims to develop low-cost materials for Nd sorption and optimize its recovery from viable alternative sources. This research evaluates the effectiveness of manganese ferrite nanoparticles ($MnFe_2O_4$) in removing Nd from a simulated NdFeB magnet leachate is evaluated. Through this approach, this study seeks to introduce $MnFe_2O_4$ nanoparticles as an efficient method for removing and recovering Nd from highly contaminated and complex solutions.

2. Materials and methods

2.1. Materials and reagents

All reagents were obtained from certified suppliers and used without further purification. Stock solutions of Nd (1000 mg/L), Dy (1000 mg/L), and Pr (1000 mg/L) were obtained from Inorganic Ventures™, while Al (1000 mg/L), Co (1000 mg/L), Ni (1000 mg/L), and Zn (1000 mg/L) were provided by Merck. Ferrous sulphate heptahydrate ($FeSO_4{\cdot}7H_2O$, >99 % purity) was purchased from Panreac, and manganese sulphate monohydrate ($MnSO_4{\cdot}H_2O$, >99 % purity) from Merck. All stock solutions were prepared in a 2–5 % HNO_3 solution. HNO_3 (65 % *v*/v) and NaOH (>98 % purity) were obtained from Merck. Ultrapure water (Milli-Q, 18 MΩ cm^{-1}) was produced in a Millipore Integral 10 system. The salt used for artificial saline solutions was sourced from Tropic Marine Centre (Tropic Marin), with its composition detailed by Atkinson et al. [33] (Supplementary Material, Table S1). Salinity was measured using a WTW series 720 multiparameter device. Glassware was washed with ultrapure water, soaked in HNO_3 (25 % *v*/v) solution for at least 24 h, and then rinsed with ultrapure water before use.

2.2. Synthesis and characterization of $MnFe_2O_4$ nanoparticles

$MnFe_2O_4$ nanoparticles were prepared following the co-precipitation method as previously described by Tavares et al. [25]. Briefly, KOH (34 mmol) and KNO_3 (15 mmol) were dissolved in 25 mL of ultrapure water previously flushed with N_2, heated to 60 °C under N_2, and mechanically stirred at 500 rpm. After total dissolution, an aqueous solution of 10 mL of $MnSO_4{\cdot}H_2O$ (6 mmol) and 15 mL of $FeSO_4{\cdot}7H_2O$ (11 mmol) was added dropwise, and the mixture was then mechanically stirred at 700 rpm. The reaction continued for 30 min before being heated to 90 °C in an oil bath, under N_2 without stirring, for 4 h. The black product was magnetically separated, rinsed with deionised water and ethanol, and subsequently dried at 40 °C. More details on procedures and reagents are described by Tavares et al. [25].

The nanoparticles were thoroughly characterised using various techniques. Transmission electron microscopy (TEM) was utilised to determine the morphology and particle size of the material, employing a Hitachi H-9000 TEM microscope operated at 300 kV. The specific surface area was assessed through Brunauer-Emmett-Teller (BET) analysis, using N_2 adsorption/desorption measurements conducted on a Gemini V2.0 Micromeritics instrument.

The crystalline structure of the nanoparticles was determined using X-ray powder diffraction analysis. The measurements were performed on the powdered samples with a Philips Analytical PW 3050/60 X'Pert PRO diffractometer operating in θ/2θ configuration. The instrument was equipped with an X'Celerator detector and automated data collection was managed through X'Pert Data Collector v2.0b software. Monochromatized Cu Kα radiation (wavelength λ = 1.54056 Å) was utilised under operating conditions of 45 kV and 40 mA.

Fourier Transform Infrared (FT-IR) spectrum was recorded with a Mattson 7000 spectrometer at a resolution of 4 cm^{-1}, using a horizontal attenuated total reflectance (ATR) cell. Magnetization and zeta potential measurements were also performed. Direct current (dc) magnetization susceptibility was measured across a temperature range of 10 to 300 K under an applied field H_{app} = 50 Oe, following initial cooling in the absence of the field and in the presence of H_{app}. Additionally, magnetization as a function of the applied field was measured at 300 K. These measurements were performed using an MPMS 5 s (Quantum Design) magnetometer equipped with a Reciprocal Sample Measurement system. Detailed methodologies for each one of these techniques can be found in previous studies [22,25].

2.3. Experimental design and response surface methodology

Sorption experiments were conducted to assess the efficiency of

$MnFe_2O_4$ nanoparticles in removing Nd from spiked ultrapure water. The experiments were performed in Schott flasks (150–250 mL) at a constant temperature of 20 °C with continuous mechanical agitation using a glass rod. Working solutions were prepared by adding a volume of the commercial stock solution of Nd to ultrapure water. To evaluate the effect of salinity, solutions with salinities of 10 and 20 were created by adding approximately 10 and 20 g of Tropic Marin salt to 1 L of ultrapure water, respectively. Different doses of $MnFe_2O_4$ nanoparticles were introduced into the Nd-spiked solutions, and the suspensions were briefly placed in an ultrasonic bath to ensure proper disaggregation and dispersion of the nanoparticles. This moment marks the beginning of the experiment (t_0). Control solutions (without sorbent) were run concurrently with each experiment to monitor potential Nd losses or contamination. Aliquots were taken at predetermined time intervals (up to 48 h), and $MnFe_2O_4$ nanoparticles were separated magnetically using an external magnet. The samples were then acidified to a pH < 2 and stored at 4 °C for later characterization.

The experimental design followed a Box-Behnken approach, a three-level factorial design (−1, 0, +1, where 0 is the central point of the experiment) already applied in REEs' sorption studies [34]. To improve the model's precision, five replicates of the central point were conducted. The three factors under study were sorbent dose (250, 625, and 1000 mg/L), initial Nd concentration (1, 25.5, and 50 μmol/L), and salinity (0, 10, and 20). The tested concentrations simulate a dilution ranging from 7 to 700 times that of a permanent magnet leachate [17,18]. The detailed experimental conditions are provided in Table 1. An additional experiment was conducted to validate the ideal conditions predicted by the model. In this experiment, a nanoparticle dose of 1000 mg/L and an Nd concentration of 20 μmol/L were used, with salinities of 0 and 20, at a pH of 6. These conditions were selected to test the accuracy of the model and its applicability under both low- and high-salinity scenarios.

Response surfaces were generated using Design-Expert V13 software from StatEase®. To develop the response surfaces, the linear, quadratic, and combined effects of each variable were modeled as a second-order polynomial and calculated using Eq. 1:

$$Y = \beta_0 + \sum_{i=1}^{k} \beta_i X_i + \sum_{i=1}^{k} \beta_{ii} X_i^2 + \sum_{i<j}^{k} \beta_{ij} X_i X_j \quad (1)$$

where Y is the value of the response variable under study, β_0 is a constant, β_i is the linear coefficient, β_{ii} is the quadratic coefficient, β_{ij} is the interaction coefficient, and $X_i, X_j, \ldots, X_k$ are the coded values of the independent variables, which were calculated according to Eq. 2:

$$X_k = \frac{x_k - x_0}{\Delta x_k} \quad (2)$$

Table 1
Experimental design matrix with the description of each experimental condition.

Experiment	Nd initial concentration (μmol/L)	Salinity	Sorbent dose (mg/L)
1	25.5	10	625
2	25.5	20	250
3	25.5	0	1000
4	50	0	625
5	1	0	625
6	1	20	625
7	25.5	10	625
8	25.5	10	625
9	1	10	250
10	25.5	0	250
11	50	10	250
12	25.5	20	1000
13	25.5	10	625
14	50	10	1000
15	1	10	1000
16	50	20	625
17	25.5	10	625

where X_k is the coded value of the independent variable x_k, x_0 is the value of the variable at the central point, and Δx_k is the phase shift between levels for variables. The significance of each effect was evaluated with ANOVA and only significant effects ($p < 0.05$) were considered in Eq. 1. Response surfaces were calculated to determine the removal percentages (R, %) for Nd in the solution, with the results representing the removal achieved after 6 and 24 h. The removal efficiency was calculated using Eq. 3:

$$R(\%) = \frac{(C_0 - C_t)}{C_0} \times 100 \quad (3)$$

where C_0 is the Nd initial concentration (μmol/L) and C_t is the Nd concentration (μmol/L) after 6 and 24 h.

Considering that all the elements removed from the solution were adsorbed onto the nanoparticles, the amount of Nd per mass of sorbent (q_t, mg/g) was calculated based on Eq. 4, where m (g) is the mass of sorbent added and V (L) is the volume of the solution. The other variables have the same meanings as described above:

$$q_t = \frac{(C_0 - C_t)}{m} \times V \quad (4)$$

2.3.1. Sorption kinetics on the removal of Nd by $MnFe_2O_4$ nanoparticles

A subsequent series of experiments was carried out to examine the sorption kinetics. These experiments were conducted using the central point condition of the Box-Behnken design, which included a Nd concentration of 25.5 μmol/L, a salinity of 10, and a sorbent dose of 625 mg/L. The experiments were performed in 250 mL Schott flasks, and control solutions were also analysed to ensure the viability of the results. Aliquots were collected at time intervals of 0, 15, 30 min, 1, 3, 6, 24, and 48 h acidified up to pH < 2 and analysed by Inductively Coupled Plasma Optical Emission Spectroscopy (ICP-OES). The sorption kinetics were examined by fitting the experimental data to three different kinetic models: Lagergren's Pseudo-First-Order (PFO) model (Eq. 5) [35], Ho's Pseudo-Second-Order (PSO) model (Eq. 6) [36], and Elovich model (Eq. 7) [37]. These three models are based on reaction kinetics and treat the sorption process comprehensively. The PFO model suggests that the rate of sorption is directly proportional to the difference between the sorption capacity and the available sorbent, making it particularly relevant for systems where the primary limitation is the availability of sorption sites. Conversely, the PSO model incorporates chemical interactions between the sorbent and sorbate, making it more appropriate for systems with high sorption capacity and where chemisorption plays a significant role. The Elovich model, while also addressing chemisorption, introduces the concept of site heterogeneity, assuming that different sorption sites exhibit varying activation energies for sorption.

$$q_t = q_e\left(1 - e^{-k1_t}\right) \quad (5)$$

$$q_t = \frac{q_e^2 k_2 t}{1 + q_e k_2 t} \quad (6)$$

$$q_t = \frac{1}{\beta} ln(1 + \alpha\beta t) \quad (7)$$

where q_t is the expected Nd concentration in $MnFe_2O_4$ nanoparticles at time t, q_e (mg/g) represents the equilibrium concentration predicted by the model, k_1 (1/h) corresponds to the PFO constant, k_2 (g/μg h) is the PSO constant, α denotes the initial sorption rate (μg h/g), and β is the desorption constant (g/μg).

2.3.2. Equilibrium sorption isotherm of Nd on $MnFe_2O_4$ nanoparticles

To investigate the sorption equilibrium of Nd onto manganese ferrite nanoparticles, equilibrium studies were conducted by contacting 200 mg/L of nanoparticles with varying Nd concentrations (1, 10, 50, and 100 μmol/L) for 48 h, based on previous studies indicating that

equilibrium was reached within this timeframe. The experiments were conducted at pH 6, a value commonly observed in real effluent solutions. Additionally, the characterization of the nanoparticles revealed that the zeta potential was positive at pH 4 and negative at pH 6. This behaviour suggests that, at pH 6, the nanoparticle surface is predominantly covered with negatively charged species, which exhibit a strong affinity for binding positively charged species such as Nd. Consequently, sorption experiments at pH 6 are particularly relevant, as this pH promotes the efficient removal of Nd from aqueous media. After the 48-h contact interval, the solutions were acidified to a pH below 2 and analysed for Nd content by ICP-OES. Equilibrium models are used to describe a sorbent's sorption capacity and to understand of the sorption mechanisms, surface properties, and affinity of the sorbent under isothermal conditions. The experimental data were fitted to three common isotherm models: Freundlich (Eq. 8) [38,39], Langmuir (Eq. 9) [38,39] and Sips (Eq. 10) [40]. Each model offers distinct insights: the Freundlich isotherm describes adsorption on heterogeneous surfaces without a saturation point; the Langmuir isotherm assumes monolayer adsorption on homogeneous surfaces; and the Sips isotherm combines aspects of both, describing adsorption on heterogeneous surfaces at low concentrations and approaching Langmuir-like saturation at higher concentrations. These models provide critical insights into the adsorption capacity and surface properties of the nanoparticles, improving the ability to predict adsorption efficiency.

$$q_e = K_F C_e^{n_F} \tag{8}$$

$$q_e = \frac{q_{mL} K_L C_e}{1 + (K_L C_e)} \tag{9}$$

$$q_e = \frac{q_{mS} K_S C_e^{n_S}}{1 + (K_S C_e)^{n_S}} \tag{10}$$

where K_L (L/μmol) and q_{mL} (μmol/g) are the Langmuir constant and sorption capacity, respectively; K_F (L/g) and n_F are the Freundlich constant and heterogeneity factor, respectively; and K_S (L/μmol), q_{mS} (μmol/g), and n_S are the Sips constant, sorption capacity, and heterogeneity criteria, respectively.

2.3.3. Simulated leachate from permanent magnets

The sorption efficiency of $MnFe_2O_4$ nanoparticles for removing REEs, specifically Dy, Nd, and Pr, was assessed using a simulated leachate solution derived from magnet scrap leaching. This solution contained a mixture of nine metals: Al, Co, Dy, Fe, Mn, Nd, Ni, Pr, and Zn (Table 2). The leachate was prepared as described by Brewer et al. [17] and Brião et al. [18]. Due to the high concentrations of certain elements, particularly Fe at 406 mg/L and Nd at 107 mg/L, a nanoparticle dose of 15 g/L was chosen to ensure effective Nd sorption. The sorption process was carried out under mechanical agitation for 24 h at a pH of 3.5. The use of acidic pH conditions could lead to the leaching of the nanoparticles, however, Pinto et al. [32] investigated the reusability of $MnFe_2O_4$ nanoparticles through multiple sorption/desorption studies, where the results regarding sorption efficiency showed no decrease after five uses, with efficiency being maintained for each element across all cycles. After five uses, the Nd efficiency was 92 %, demonstrating that the $MnFe_2O_4$ nanoparticles can be reused at least up to five times without leaching occurring in acidic media. The concentrations of REEs were measured using ICP-OES.

Table 2
Composition of the simulated leachate solution of a magnet [17,18].

Elements	Concentration (μmol/L)
Al	34
Co	120
Dy	48
Fe	7270
Mn	15
Nd	740
Ni	26
Pr	260
Zn	430

2.3.4. Desorption experiments

Desorption experiments were conducted at room temperature (20 °C) using 5 mg of $MnFe_2O_4$ nanoparticles that had previously interacted with a solution simulating leachate from permanent magnets. These nanoparticles were exposed to 10 mL of 0.01 mol/L HNO_3, selected as the desorption agent. Desorption was carried out for 24 h. The nanoparticles were then magnetically separated, and the liquid samples were analysed by ICP-OES. Desorption efficiency was determined using Eqs. 11 and 12:

$$C_{theoretical} = \frac{q_t \times m}{V} \times 1000 \tag{11}$$

$$\text{Recovery } (\%) = \frac{C}{C_{theoretical}} \times 100 \tag{12}$$

where $C_{theoretical}$ (mg/L) represents the theoretical concentration of the chemical element in the solution, q_t (mg/g) is the amount of the element sorbed by the sorbent, m (g) is the mass of sorbent used in the desorption process, V (mL) is the volume of the acidic desorption solution, and C (mg/L) is the concentration of the chemical element measured after desorption.

2.4. Neodymium quantification

The quantification of elements in liquid samples was performed by ICP-OES (Jobin Yvon Activa M (radial configuration) equipped with a peristaltic pump and a Burgener nebuliser). Only calibration curves with a correlation coefficient >0.9995 were accepted. Control standards were analysed at regular intervals to ensure that the quality and accuracy criteria were continuously met. The error associated with each standard was <10 % and the lowest calibration standard was considered the limit of quantification. The range of the calibration standards varied from 10 to 500 μg/L.

After the sorption process, the quantification of Nd and other elements in the nanoparticles was performed, requiring the acid digestion of the materials for analysis. In the digestion procedure, 20 mg of nanoparticles were weighed into Teflon containers. The nanoparticles were then digested in a CEM MARS 5 microwave using 1 mL of 65 % HNO_3 for 20 min, at 170 °C. The digests were collected in 25 mL polythene containers, where the volume was topped up with ultrapure water. The samples were then analysed by ICP-OES. To ensure the quality of the method, a blank (Teflon container with only HNO_3) was carried out in parallel, which was always below the limit of quantification (10 μg/L).

3. Results and discussion

3.1. Characterization of manganese ferrite nanoparticles

A previous study detailed the synthesis and characterization of $MnFe_2O_4$ nanoparticles for sorption applications [22]. A typical TEM image of the $MnFe_2O_4$ nanoparticles is shown in Fig. 1A, revealing spherical particles with an average diameter of 75 ± 15 nm. Furthermore, these nanoparticles exhibited a BET surface area of 39.2 m^2/g and a pore volume of 0.11 cm^3/g. Magnetic hysteresis analysis confirmed ferrimagnetic behaviour, with a specific saturation magnetization of 48.1 emu/g (Fig. 1B). Zeta potential measurements showed a value of 16.6 mV at pH 4 and − 23.3 ± 0.9 mV at pH 6 (n = 5), indicating a negatively charged surface at pH 6, which enhances the nanoparticles' affinity for adsorbing positively charged species like Nd^{3+}. The X-ray

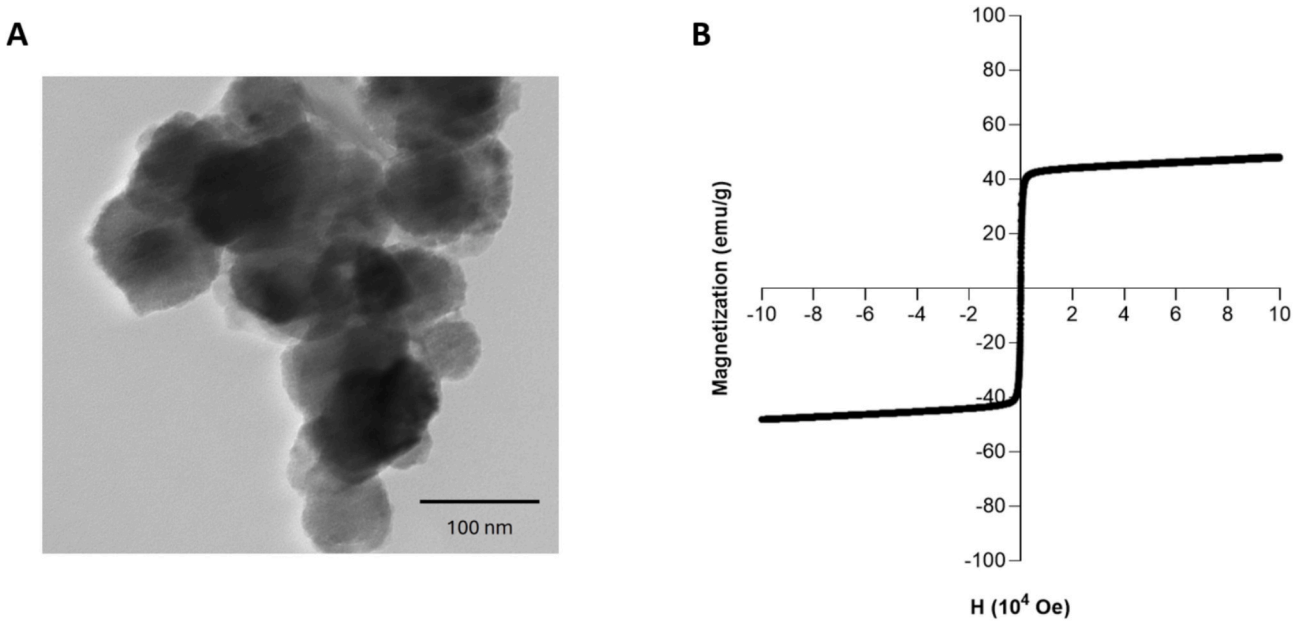

Fig. 1. TEM image (A) and magnetization curve of $MnFe_2O_4$ nanoparticles, as a function of the magnetic field measured at 300 K (B).

diffraction (XRD) patterns of the $MnFe_2O_4$ nanoparticles, shown in Fig. 2, display characteristic peaks corresponding to the crystalline spinel structure of $MnFe_2O_4$, as indexed by the JCPDS – International Centre for Diffraction Data (PDF card 01–071-4919). The FT-IR spectrum of $MnFe_2O_4$ is represented in Fig. 3. The vibrational band observed at 537 cm^{-1} corresponds to metal–O stretching vibrations within the lattice, while the band at 1095 cm^{-1} is associated to metal –OH and metal $–OH_2$ stretching vibrations, indicative of water sorption on the oxide surface [25]. The band at 1643 cm^{-1} is attributed to H–O–H bending vibrations, arising from molecular water adsorbed or incorporated into the crystalline lattice. The broader band at 3369 cm^{-1} is linked to O—H stretching modes of chemisorbed water.

3.2. Response surface methodology

Control experiments using ultrapure water with Nd and without sorbent showed negligible changes in Nd concentration, confirming that losses from precipitation or contamination did not impact the sorption process.

The response surfaces for Nd removal, depicted in Fig. 4, show metal removal as a function of Nd concentration and sorbent dose across varying salinity levels (0, 10, and 20) after 6 and 24 h. The model fit,

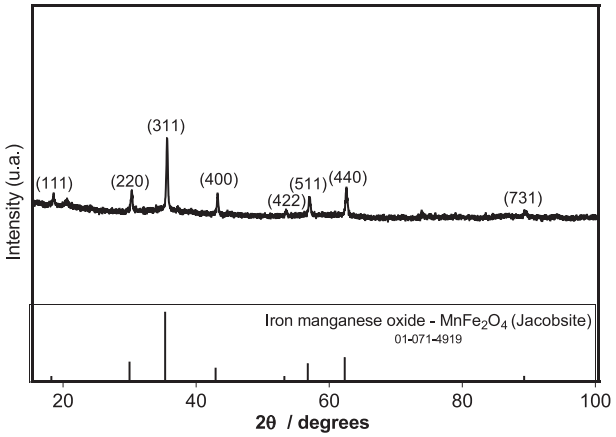

Fig. 2. Powder X-ray diffraction of $MnFe_2O_4$ particles.

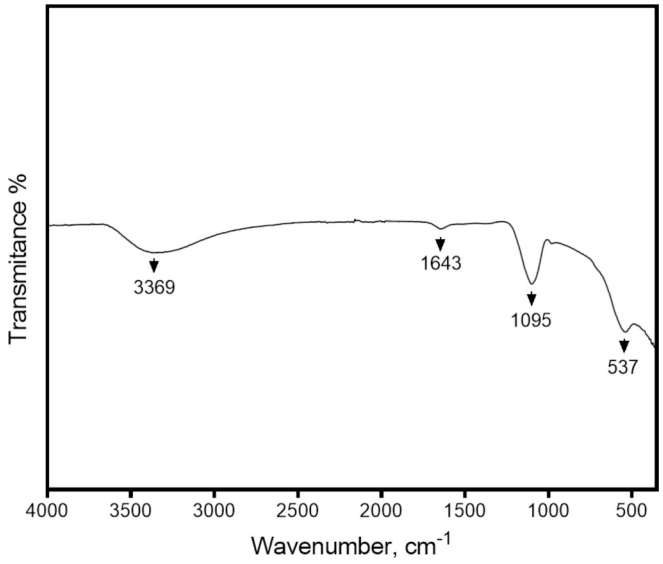

Fig. 3. Infrared spectrum of $MnFe_2O_4$ nanoparticles.

with correlation coefficients (R^2) of 0.8420 and 0.8554 for 6 and 24 h, respectively, provided reasonable estimates of the response, demonstrating a good fit [41,42].

A significant relationship between salinity and Nd removal efficiency was observed. After 6 h, the maximum removal efficiency of 94.5 % was achieved at no salinity, using a sorbent dose of 1000 mg/L and an Nd concentration of 23 μmol/L. After 24 h, the maximum removal efficiency increased to 97.2 % under similar conditions. However, as salinity increased, the efficiency of Nd removal decreased, with maximum removal rates at salinity 10 reaching 76.5 % after 6 h and 83.8 % after 24 h. At the highest salinity level (20), maximum removal rates were 70 % after 6 h, rising to 77.7 % after 24 h. These findings highlight that while Nd removal improved with higher sorbent doses and lower salinity, the concentration of Nd for maximum removal varied between 23 and 25.5 μmol/L. Despite this, sorption was not completely inhibited at higher salinities and the sorbent remained effective, suggesting that $MnFe_2O_4$ nanoparticles can remove Nd in saline

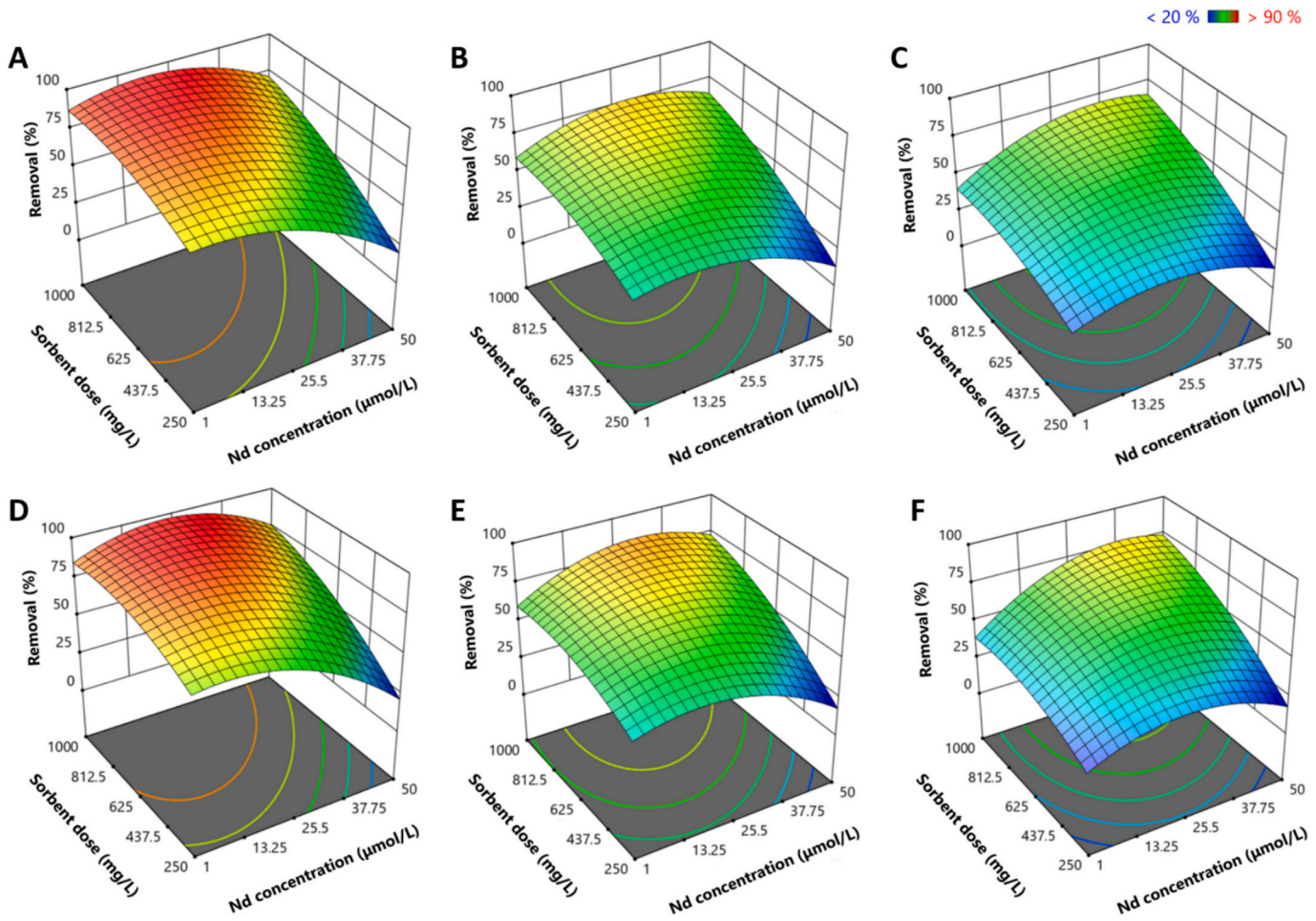

Fig. 4. Response surfaces obtained for the removal of Nd by $MnFe_2O_4$ nanoparticles at 6 h (A to C) and 24 h (D to F) of contact time. The removals at salinity 0 (A and D), salinity 10 (B and E), and salinity 20 (C and F) are represented.

environments.

It is well established that increased ionic strength, such as from NaCl, can significantly reduce sorption efficiency due to competition for active sites and the barrier effect posed by Na^+ ions. In this study, this effect is evident, as increasing salinity decreases the removal efficiency by around 20 %, even at the highest nanoparticle dose, compared to the efficiency observed at zero salinity. This susceptibility to high ionic strength had not been reported in previous research. Studies by Pinto et al. [32] and Tu et al. [43] showed that $MnFe_2O_4$ nanoparticles maintained their capacity to remove REEs even in the presence of high NaCl concentrations. However, the difference in removal rates between those reported in previous studies and those determined in the present study may be attributed to variations in experimental conditions. In this study, the saline matrix is more complex than a simple NaCl solution. The presence of additional major cations in the salt used to prepare the saline solutions (such as Na^+, K^+, Mg^{2+}, and Ca^{2+}) likely contributes to the more pronounced decline in sorption efficiency compared to earlier studies. This approach, however, is a more realistic assessment of $MnFe_2O_4$ sorption efficiency in saline aquatic environments, which are typically more complex. Despite the reduction in efficiency with increasing salinity, the results showed that a maximum removal rate of 83.8 % was achieved for a salinity of 10 and 77.7 % for a salinity of 20, after 24 h. These finding show that manganese ferrite nanoparticles are still effective for removing REEs from saline matrices.

Table 3 shows that nearly complete Nd removal (94.5 %) was achieved after 6 h, using an initial Nd concentration of approximately 20 µmol/L and the highest nanoparticle dose (1000 mg/L). The optimal conditions (1000 mg/L nanoparticle dose and salinity of zero) remained consistent across both time intervals, suggesting that these parameters are well-defined. Thus, the ideal conditions for effective Nd removal include a nanoparticle dose of 1000 mg/L, a salinity of zero, and an initial Nd concentration of 20 µmol/L at a pH 6, with 24 h required for near-complete removal. Experimental validation under these conditions (Table 3) produced results closely aligned with the model's predictions for salinity 0. Although Nd removal was marginally lower than expected, the relative errors remained within 5 %, confirming the model's reliability. Overall, these optimized conditions, achieving at least 90 % Nd removal from aqueous solutions, are effective for Nd extraction using manganese ferrite nanoparticles, demonstrating significant potential for industrial applications.

Table 3
Validation of the optimal conditions predicted by the model – comparison between the Nd removal percentages predicted by the model and those obtained in experimental assays.

Time (h)	pH	Nd concentration (µmol/L)	Salinity	Nanoparticles dose (mg/L)	Removal expected (%)	Removal obtained (%)	Relative error (%)
6	6	20	0	1000	94.5	90	4
24					97	93	5

3.2.1. Sorption kinetics of Nd by $MnFe_2O_4$ nanoparticles

Fig. 5 shows the percentage of Nd removed during a 48-h contact interval with $MnFe_2O_4$ nanoparticles, under the following conditions: salinity of 10, a sorbent dose of 625 mg/L, and an initial Nd concentration of 25.5 μmol/L at pH 6. These parameters represent the central point of the Box Behnken design used for optimization studies. Samples were collected at various time intervals from 0 to 48 h. The data shows a rapid increase in Nd removal during the first 6 h, followed by a slower rate of removal, ultimately reaching a plateau at 24 h. The larger standard deviations (<17 %) observed during the initial 6-h interval were primarily due to variability in the magnetic separation process, which had to be performed quickly to avoid disrupting the kinetic studies. At later time points, these deviations (<9 %) decreased as slower separation became feasible.

To investigate the sorption kinetics, the Nd removal data was fitted to three kinetic models: PFO, PSO, and Elovich (Fig. 6). Table S2, from Supplementary Material, presents the fitting parameters for the kinetic models. The Elovich model provided the best fit, with the highest R^2 values, suggesting that chemisorption, such as ion exchange [7,31], is the dominant mechanism. These models accounts for the heterogeneity of the sorption sites, implying varying activation energies. As shown in Fig. 6, the q_t value is higher for the Elovich model, indicating greater enrichment of the sorbent. However, the kinetics are slower compared to the PFO model for example, likely because the Elovich model describes chemical interactions that dominate during prolonged sorption periods, where the sorption rate progressively decreases and does not account for simultaneous desorption, as often occurs in ion capture within porous solids [44]. Consequently, the Elovich model is more applicable in the early stages of sorption, when the system is far from equilibrium. The low standard deviation value, $S_{x/y}$, further supports the Elovich model's superior fit, as it demonstrates the least variability in residuals, indicating a more accurate representation of the experimental data compared to the other models.

3.2.2. Sorption isotherms of Nd by $MnFe_2O_4$ nanoparticles

The sorption capacity of $MnFe_2O_4$ nanoparticles for Nd was evaluated at varying initial Nd concentrations (1, 10, 50, and 100 μmol/L) using a fixed sorbent dose of 200 mg/L at pH 6, after a 48-h contact interval. As shown in Fig. 7, the sorption capacity of the nanoparticles increases with rising Nd concentrations, reaching a maximum of 8 mg/g at 50 and 100 μmol/L. This saturation plateau indicates that the nanoparticles have reached their maximum sorption capacity, beyond which no significant increase in Nd uptake occurs, despite the higher availability of Nd. This behaviour suggests that the sorbent sites are fully occupied at these higher concentrations, limiting further sorption.

To better understand the sorption equilibrium dynamics, the experimental data were fitted to the Freundlich, Langmuir, and Sips isotherm

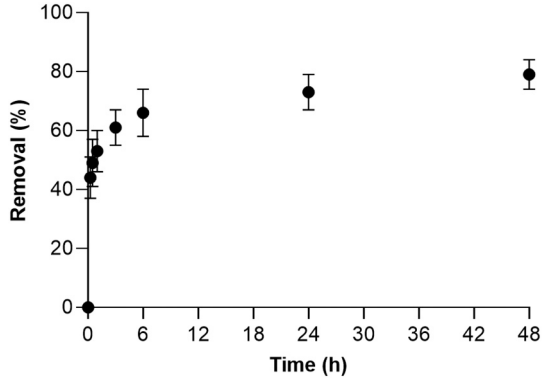

Fig. 5. Removal percentages (%) of neodymium by $MnFe_2O_4$ along 48 h of contact time. Experimental conditions: sorbent dose of 625 mg/L, initial Nd concentration of 25.5 μmol/L, and salinity of 10, for pH 6.

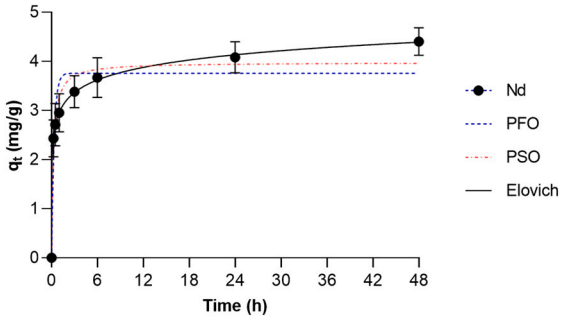

Fig. 6. Curve fittings of three kinetic models (PFO, PSO, and Elovich) to q_t values.

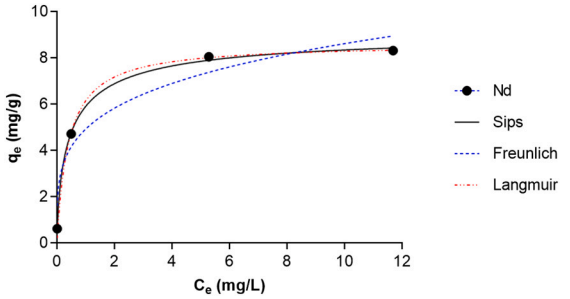

Fig. 7. Neodymium (Nd) sorption isotherms on manganese ferrite nanoparticles (sorbent dose of 200 mg/L), after 48 h at pH 6.

models. As shown in Fig. 7 and Table S3, from Supplementary Material, the Sips model provided the best fit, as evidenced by its higher R^2 values and lower standard deviation ($S_{x/y}$), reflecting its superior accuracy in describing the experimental data. The Sips model, which assumes a surface with homogeneous energetic sites and cooperative sorbante-sorbate interactions, accurately describes the sorption process, particularly by transitioning from Freundlich behaviour at low equilibrium concentrations (C_e) to Langmuir-type monolayer sorption at high C_e. This versatility allows the Sips model to describe the behaviour of $MnFe_2O_4$ nanoparticles across a wide range of Nd concentrations with high precision.

The experimental maximum sorption capacity was 8 mg/g, with a slight error of 13.2 % when compared to the model-predicted capacity of 9.218 mg/g. This small discrepancy falls within acceptable limits, confirming the validity and reliability of the sorption process. Given the close alignment between experimental and predicted values, it can be assumed that the maximum sorption capacity of the nanoparticles is 8 mg/g. Additionally, the Sips constant of 2.207 suggests that sorbent saturation occurs at lower C_e values [18]. These findings highlight the applicability of the Sips model in predicting the sorption performance of $MnFe_2O_4$ nanoparticles for Nd, particularly in systems with varying concentrations.

3.2.3. Simulated leachate from permanent magnets

Fig. 8 illustrates the sorption behaviour of $MnFe_2O_4$ nanoparticles for each metal present in the simulated leachate from a permanent magnet. The sorption efficiency (%) follows the increasing order of: Fe > Dy > Nd > Pr > Zn > Co > Ni > Al. The $MnFe_2O_4$ nanoparticles exhibited non-selective sorption of the ions in the simulated leachate, showing no particular preference was observed for any specific metal. The nanoparticles effectively removed nearly all elements, not just REEs. Since Mn is part of the nanoparticles' composition and was partially leached due to the acidic nature of the solution, it is not represented in the results despite being present in the initial leachate. Fe, the primary component of the nanoparticles, displayed the highest removal efficiency (99.8 %),

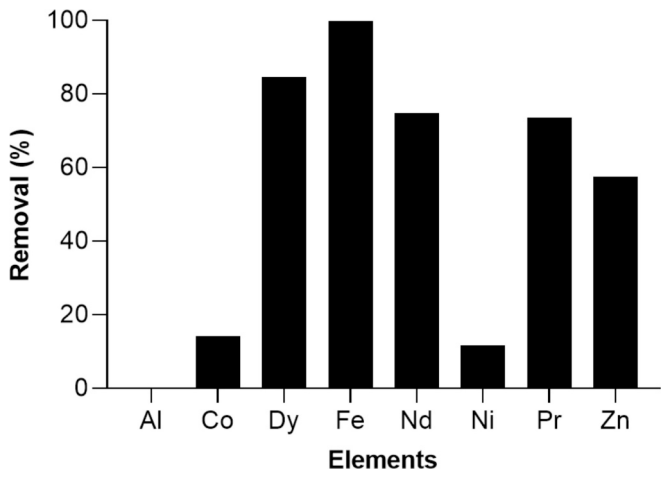

Fig. 8. Removal percentages (%) of the elements present in a synthetic solution simulating the dissolution of a magnet after 24 h (sorbent dose 15 g/L and pH 3.5).

indicating that, unlike Mn, the Fe within the nanoparticles remained intact and was not leached even under acidic conditions.

For the removal of Nd, Dy, and Pr (some of the most economically valuable elements in the simulated leachate) the nanoparticles achieved removal efficiencies of 74.8 % for Nd, 84.7 % for Dy, and 73.5 % for Pr. The initial concentrations of these elements in the solution were 740 µmol/L (107 mg/L) for Nd, 48 µmol/L (8 mg/L) for Dy, and 260 µmol/L (37 mg/L) for Pr. It was anticipated that the sorbent would be more enriched in Nd due to its higher concentration in the leachate (Fig. 9). While achieving optimal removal efficiency is ideal, the current conditions do not fully mirror the real industrial environments. Therefore, these results obtained from a solution containing a mixture of metals, provide a more realistic reflection of industrial conditions. In this context, the removal percentages of the REEs are considered favourable.

Fig. 9 compares the predicted and observed sorption quantities of Dy, Nd, and Pr by manganese ferrite nanoparticles, using a material concentration of 15 g/L in this trial. The three elements exhibited an error margin of around 20 % between the expected and observed q_t values, suggesting that increasing the nanoparticle dose to 17–20 g/L may be necessary for complete Nd removal. This adjustment in nanoparticle dosages has significant implications for the scalability of the removal process. If the required amount of nanoparticles is too high, it could compromise the economic viability of the method by increasing operational and logistical costs, unless the nanoparticles can be produced at a very low cost. Therefore, it is crucial to carefully assess the relationship between nanoparticle dose and removal efficiency to ensure that the process remains effective, scalable, and economically viable. The relatively high removal percentages obtained in this study indicate strong potential for industrial applications in recovering Nd from permanent magnets. However, further optimization is needed for future trials involving real magnet dissolution matrices and larger-scale sorption assays.

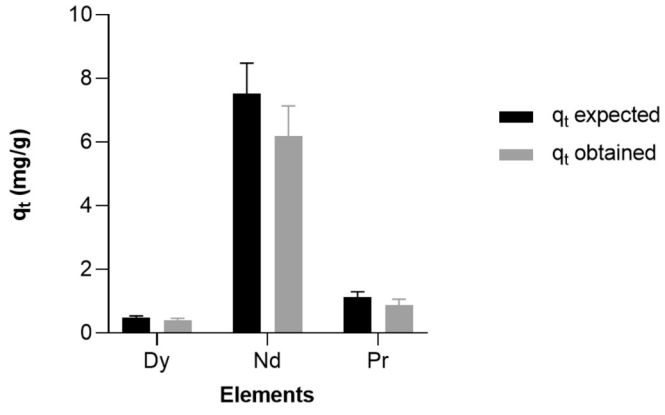

Fig. 9. Comparison of the amount of element sorbed by the manganese ferrite nanoparticles (q_t), both expected and obtained for the elements Dy, Nd, and Pr.

3.2.4. *Desorption experiments*

Nd, Dy, and Pr were analysed in the desorption experiments. Table 4 presents the desorption efficiencies for each element, expressed as percentages. The data show that all elements can reach 100 % recovery within 6 h, indicating that extending the contact time to 24 h is unnecessary, as the same behaviour is observed at both time points. Since desorption percentages for all elements exceed 80 %, the concentration of HNO_3 has minimal effect on the desorption efficiency for these three elements.

Overall, effective desorption is achieved for all elements, which is promising for both the potential reuse of manganese ferrite nanoparticles and the recovery of these elements. The results also demonstrate that diluted HNO_3 is effective for desorption. Nonetheless, further research is needed to determine the minimum concentration of the HNO_3 solution required for desorption and to evaluate the sorption efficiency of the recycled material.

3.3. *Performance of $MnFe_2O_4$ nanoparticles for Nd removal: A comparative assessment*

A review of the literature reveals that most studies investigating Nd removal from water using different sorbents are conducted in simplified matrices. These typically involve initial Nd concentrations between 200 and 250 mg/L, pH levels ranging from 5 to 6, sorbent doses of 1 to 5 g/L, and contact times of 1 to 6 h [45–52]. Several studies have explored the application of manganese ferrite nanoparticles for contaminant removal from water. These studies often employ initial Nd concentrations around 500 mg/L, with pH levels between 6 and 7, sorbent doses below 1 g/L, and contact times ranging from 20 min to 1 h [7,22,24,31,53–56]. While initial Nd concentrations in these studies vary slightly (200 to 500 mg/L), such high levels can present challenges for achieving efficient removal. This study, though broadly consistent with these parameters, distinguishes itself by examining the impact of salinity in a real marine environment using actual marine salt. This is in contrast to much of the existing research, which typically employs NaCl to simulate salinity. Furthermore, the present study investigates a more complex solution derived from the dissolution of permanent magnets, offering valuable insights into Nd removal under more realistic and challenging conditions.

When comparing the findings of this study with previous research, notable differences in sorption capacities emerge. For instance, Durán et al. [53] reported a maximum sorption capacity of 44.29 mg/g for Nd removal using $MnFe_2O_4$-chitosan nanoparticles in deionised water with a contact time of 250 min. In contrast, Liu et al. [31] achieved much higher sorption capacities, exceeding 1000 mg/g for La and Ce removal using modified $MnFe_2O_4$ nanoparticles, with much shorter contact times of 30 min. Similarly, Ghobadi et al. [7] observed high sorption capacities with $MnFe_2O_4$-GO nanoparticles, reporting up to 1001 mg/g for La and 982 mg/g for Ce in only 20 min.

Table 4
Recovery percentage (%) of Dy, Nd, and Pr desorption from manganese ferrite nanoparticles, after 1, 6, and 24 h contact time.

Time (h)	[HNO_3] (mol/L)	Recovery (%)		
		Dy	Nd	Pr
1	0.01	84	85	84
6		100	100	100
24		100	100	100

While previous studies have demonstrated that modifying nanoparticles can significantly enhance sorption performance, this study highlights the use of unmodified nanoparticles as a more sustainable alternative. Although modified nanoparticles are highly effective, their production often involves more complex and less environmentally friendly processes. In contrast, unmodified manganese ferrite nanoparticles still achieved high removal efficiencies, exceeding 90 % in freshwater and 70 % in saline water, even in more complex solutions like magnet leachate. This highlights their potential as a simpler and more practical solution, particularly in real-world applications where competing ions are present.

In the studies conducted by Brião et al. [18] and Dudarko et al. [57], both explored REE sorption from a simulated NdFeB magnet leachate in batch mode under similar experimental conditions, differing primarily in pH and sorbent dosage. Dudarko et al. [57] adjusted the leachate pH to precipitate iron, thereby reducing competition between iron and REEs during sorption, whereas Brião et al. [18] did not, a situation similar to the present study. Nevertheless, the sorption capacities reported in these studies were higher than those achieved here. Dudarko et al. [57] reported a sorption capacity (qe) of 1.19 mmol/g (171.6 mg/g) for Nd, while Brião et al. [18] observed a qe of 1.4 mmol/g (201.9 mg/g). In this study, the maximum sorption capacity for Nd removal was considerably lower, reaching only 8 mg/g after 48 h. This reduced capacity, compared to values reported in the literature, can be attributed to the more complex and realistic conditions of the experiments. Unlike previous studies, which typically employed simpler matrices such as deionised or ultrapure water, this study focused on a real saline environment, with high salinity and the presence of competing ions. These factors likely increased competition for sorption sites, resulting faster saturation of the material.

Furthermore, this study examined a solution derived from the dissolution of permanent magnets, adding an additional layer of complexity compared to the ideal conditions often used in published works. These more realistic conditions make it challenging to achieve the same high sorption efficiencies reported in simpler systems, where the absence of competing ions allows for more optimal removal performance. Consequently, while the maximum sorption capacity observed in this study was lower, it reflects a more practical scenario for real-world applications. This highlights the importance of adjusting expectations when moving from controlled laboratory experiments to more complex environmental systems.

4. Conclusions

In conclusion, this study highlights the effectiveness of manganese ferrite nanoparticles as a highly efficient method for the removal of Nd from aqueous solutions. The initial experiments demonstrated the nanoparticles' strong capacity for Nd extraction from ultrapure water, while further optimisation through response surface methodology identified key factors affecting removal efficiency. Notably, nanoparticle dosage emerged as the most significant factor, with salinity negatively influencing the performance. The optimal conditions, including a nanoparticle dose of 1000 mg/L, an initial Nd concentration of 20 μmol/L, and zero salinity, achieved nearly 100 % removal after 24 h at pH 6, with experimental validation confirming over 90 % removal efficiency.

Simulation of real magnet dissolution conditions revealed removal rates exceeding 70 %, with $MnFe_2O_4$ nanoparticles displaying non-selective sorption behaviour and effectively removing a variety of elements, including REEs like Nd, Dy, and Pr. Although this lack of selectivity may require additional downstream processing steps, the potential economic and environmental impacts of such processes warrant further investigation. For sorption to become a viable alternative to conventional REE recovery methods, future studies should incorporate both pre- and post-sorption processes in their enviro-economic assessments, including tools such as Life Cycle Assessment. While the experimental conditions did not fully replicate industrial processes, the promising removal rates in complex media suggest significant potential for industrial applications, particularly in recovering Nd from permanent magnet effluents. This efficient Nd removal could also extend to other REE-rich effluents, with $MnFe_2O_4$ nanoparticles offering a sustainable solution for REE management. However, additional optimisation is necessary to improve performance under real industrial conditions, especially in large-scale sorption assays and magnet dissolution matrices.

The successful desorption experiments demonstrated the feasibility of industrial-scale recovery, with 100 % recovery achieved within just 6 h. This high desorption efficiency, coupled with the techno-economic viability of $MnFe_2O_4$ nanoparticles for recovering Nd from permanent magnet effluents, positions the material as suitable for scale-up. Optimising the desorption process is essential to improve selectivity and efficiency in larger-scale applications. Furthermore, future research should explore the reusability of $MnFe_2O_4$ nanoparticles through multiple desorption cycles, as this would reduce material synthesis costs and lower the environmental footprint of large-scale applications.

Given their removal performance, these nanoparticles show great promise as sorbents for Nd recovery from industrial leachates, supporting both economic and environmental sustainability. Future research should focus on investigating additional parameters, such as temperature, nanoparticle toxicity, optimal desorption conditions, and consecutive sorption/desorption cycles to evaluate nanoparticle recyclability. This will optimize the process and ensure its long-term effectiveness and sustainability at a larger scale.

CRediT authorship contribution statement

Joana Sousa: Writing – original draft, Validation, Investigation, Formal analysis. **Daniela S. Tavares:** Validation, Supervision, Investigation, Conceptualization. **João Pinto:** Writing – review & editing, Validation, Investigation, Formal analysis. **Bruno Henriques:** Writing – review & editing, Supervision, Methodology. **João Rocha:** Writing – review & editing, Methodology. **Tito Trindade:** Resources, Methodology. **Nuno Lapa:** Writing – review & editing. **Eduarda Pereira:** Supervision, Resources, Project administration, Funding acquisition, Conceptualization.

Declaration of generative AI and AI-assisted technologies in the writing process

During the preparation of this work the authors used ChatGPT-4 exclusively to improve the readability and language of the manuscript. After using this tool, the authors reviewed and edited the content as needed and take full responsibility for the content of the published article.

Funding

This work received financial support from PT national funds (FCT/MCTES, Fundação para a Ciência e Tecnologia and Ministério da Ciência, Tecnologia e Ensino Superior) through the CICECO-Aveiro Institute of Materials (UIDB/50011/2020 and UIDP/50011/2020), and REQUIMTE (UIDB/50006/2020 and UIDP/50006/2020).

Declaration of competing interest

The authors declare that they have no known competing financial interests or personal relationships that could have appeared to influence the work reported in this paper.

Acknowledgements

João Pinto thanks FCT/MCTES (Fundação para a Ciência e

Tecnologia and Ministério da Ciência, Tecnologia e Ensino Superior) for his PhD grant (ref. doi:10.54499/2020.05323.BD). Bruno Henriques thanks FCT (Fundação para a Ciência e Tecnologia) for funding through the Scientific Employment (Ref. 10.54499/CEECIND/03511/2018/CP1559/CT0032). Nuno Lapa thanks Fundação para a Ciência e a Tecnologia for funding LAQV-REQUIMTE (LA/P/0008/2020 DOI 10.54499/LA/P/0008/2020, UIDP/50006/2020 DOI 10.54499/UIDP/50006/2020 and UIDB/50006/2020 DOI 10.54499/UIDB/50006/2020) through national funds.

Appendix A. Supplementary data

Supplementary data to this article can be found online at https://doi.org/10.1016/j.jwpe.2025.107200.

Data availability

Data will be made available on request.

References

[1] K. Binnemans, P.T. Jones, B. Blanpain, T. Van Gerven, Y. Yang, A. Walton, M. Buchert, Recycling of rare earths: a critical review, J. Clean. Prod. 51 (2013) 1–22, https://doi.org/10.1016/j. jclepro.2012.12.037.
[2] V. Balaram, Rare earth elements: a review of applications, occurrence, exploration, analysis, recycling, and environmental impact, Geosci. Front. 10 (2019) 1285–1303, https://doi.org/10.1016/j. gsf.2018.12.005.
[3] J. Pinto, J. Sousa, D. Tavares, B. Henriques, T. Viana, N. Ferreira, J. Rocha, E. Pereira, Removal of rare-earth elements from aqueous solutions by microporous titanosilicate ETS-4, Microporous Mesoporous Mater. 357 (2023) 112606, https://doi.org/10.1016/j.micromeso.2023. 112606.
[4] N.K. Gupta, A. Gupta, P. Ramteke, H. Sahoo, A. Sengupta, Biosorption-a green method for the preconcentration of rare earth elements (REEs) from waste solutions: a review, J. Mol. Liq. 274 (2019) 148–164, https://doi.org/10.1016/j.molliq.2018.10.134.
[5] A. Golev, M. Scott, P.D. Erskine, S.H. Ali, G.R. Ballantyne, Rare earths supply chains: current status, constraints and opportunities, Res. Policy 41 (2014) 52–59, https://doi.org/10.1016/j. resourpol.2014.03.004.
[6] J. Jacinto, B. Henriques, A.C. Duarte, C. Vale, E. Pereira, Removal and recovery of critical rare elements from contaminated waters by living Gracilaria gracilis, J. Hazard. Mater. 344 (2018) 531–538, https://doi.org/10.1016/j.jhazmat.2017.10.054.
[7] M. Ghobadi, M. Gharabaghi, H. Abdollahi, Z. Boroumand, M. Moradian, MnFe2O4-graphene oxide magnetic nanoparticles as a high-performance adsorbent for rare earth elements: synthesis, isotherms, kinetics, thermodynamics and desorption, J. Hazard. Mater. 351 (2018) 308–316, https://doi.org/10.1016/j.jhazmat.2018.03.011.
[8] European Commission, Study on the Critical Raw Materials for the EU 2023 Final Report, 2023. doi:https://doi.org/10.2873/725585.
[11] A. Kumari, S.K. Sahu, A comprehensive review on recycling of critical raw materials from spent neodymium iron boron (NdFeB) magnet, Sep. Purif. Technol. 317 (2023) 123527, https://doi.org/10.1016/j. seppur.2023.123527.
[12] U.S Department of Energy, Critical Materials Assessment, 2023. https://www.energy.gov/cmm/ critical-minerals-materials-program.
[13] T. Viana, B. Henriques, N. Ferreira, C. Lopes, D. Tavares, E. Fabre, L. Carvalho, J. Pinheiro-Torres, E. Pereira, Sustainable recovery of neodymium and dysprosium from waters through seaweeds: influence of operational parameters, Chemosphere 280 (2021) 130600, https://doi.org/10.1016/j.chemosphere.2021.130600.
[14] R. Freitas, S. Costa, C.E.D. Cardoso, T. Morais, P. Moleiro, A.C. Matias, A.F. Pereira, J. Machado, B. Correia, D. Pinheiro, A. Rodrigues, J. Colónia, A.M.V.M. Soares, E. Pereira, Toxicological effects of the rare earth element neodymium in Mytilus galloprovincialis, Chemosphere 244 (2020) 125457, https://doi.org/10.1016/j.chemosphere.2019.125457.
[15] Z. Chen, Z. Li, J. Chen, P. Kallem, F. Banat, H. Qiu, Recent advances in selective separation technologies of rare earth elements: a review, J. Environ. Chem. Eng. 10 (2022) 107104, https://doi.org/10.1016/j.jece.2021.107104.
[17] A. Brewer, A. Dohnalkova, V. Shutthanandan, L. Kovarik, E. Chang, A.M. Sawvel, H.E. Mason, D. Reed, C. Ye, W.F. Hynes, L.N. Lammers, D.M. Park, Y. Jiao, Microbe encapsulation for selective rare-earth recovery from electronic waste leachates, Environ. Sci. Technol. 53 (2019) 13888–13897, https://doi.org/10.1021/acs.est.9b04608.
[18] G. de V. Brião, C.B. Lopes, T. Trindade, C.M. Silva, M.G.C. da Silva, M.G.A. Vieira, NdFeB magnet scrap valorization by leaching and recovery of rare earth metals by sorption on low-cost expanded clay, Journal of Industrial and Engineering Chemistry 131 (2024) 558–568. doi:10.10 16/j.jiec.2023.10.060.
[19] C.E.D. Cardoso, J.C. Almeida, C.B. Lopes, T. Trindade, C. Vale, E. Pereira, Recovery of rare earth elements by carbon-based nanomaterials—a review, Nanomaterials 9 (2019) 1–35, https://doi.org/10.3390/nano9060814.
[20] A.M. Younis, A.V. Kolesnikov, A.V. Desyatov, Efficient removal of La(III) and Nd (III) from aqueous solutions using carbon nanoparticles, Am. J. Anal. Chem. 05 (2014) 1273–1284, https://doi.org/10.4236/ajac.2014.517133.
[22] J. Pinto, D. Branco, L. Carvalho, B. Henriques, R. Freitas, T. Trindade, D. Tavares, E. Pereira, Influence of experimental parameters on the sorption behavior of rare earth elements on manganese ferrite nanoparticles, Environ. Technol. Innov. 32 (2023) 103432, https://doi.org/10.1016/j.eti. 2023.103432.
[23] H. Viltres, N.K. Gupta, R. Paz, R.P. Dhavale, H.H. Park, C. Leyva, S. Srinivasan, A. R. Rajabzadeh, Mercury remediation from wastewater through its spontaneous adsorption on non-functionalized inverse spinel magnetic ferrite nanoparticles, Environ. Technol. (2022) 1–15, https://doi.org/10.1080/09593330.2022.2138787.
[24] S. Kumar, R.R. Nair, P.B. Pillai, S.N. Gupta, M.A.R. Iyengar, A.K. Sood, Graphene oxide-MnFe2O4 magnetic nanohybrids for efficient removal of lead and arsenic from water, ACS Appl. Mater. Interfaces 6 (2014) 17426–17436, https://doi.org/10.1021/am504826q.
[25] D.S. Tavares, C.B. Lopes, J.C. Almeida, C. Vale, E. Pereira, T. Trindade, Spinel-type ferrite nanoparticles for removal of arsenic(V) from water, Environ. Sci. Pollut. Res. 27 (2020) 22523–22534, https://doi.org/10.1007/s11356-020-08673-9/Published.
[26] Y.J. Tu, C.F. You, M.H. Chen, Y.P. Duan, Efficient removal/recovery of Pb onto environmentally friendly fabricated copper ferrite nanoparticles, J. Taiwan Inst. Chem. Eng. 71 (2017) 197–205, https://doi.org/10.1016/j.jtice.2016.12.006.
[27] T. Tatarchuk, A. Shyichuk, Z. Sojka, J. Gryboś, M. Naushad, V. Kotsyubynsky, M. Kowalska, S. Kwiatkowska-Marks, N. Danyliuk, Green synthesis, structure, cations distribution and bonding characteristics of superparamagnetic cobalt-zinc ferrites nanoparticles for Pb(II) adsorption and magnetic hyperthermia applications, J. Mol. Liq. 328 (2021) 115375, https://doi.org/10.1016/j.molliq.2021. 115375.
[28] A. Homayonfard, M. Miralinaghi, R.H. Seyed Mohammad Shirazi, E. Moniri, Efficient removal of cadmium (II) ions from aqueous solution by CoFe 2 O 4/ chitosan and NiFe 2 O 4/chitosan composites as adsorbents, Water Sci. Technol. 78 (2018) 2297–2307. doi:10.2166/ wst.2018.510.
[29] N. Gupta, P. Pant, C. Gupta, P. Goel, A. Jain, S. Anand, A. Pundir, Engineered magnetic nanoparticles as efficient sorbents for wastewater treatment: a review, Mater. Res. Innov. 22 (2018) 434–450, https://doi.org/10.1080/14328917.2017.1334846.
[30] V. Gupta, P.J.M. Carrott, M.M.L. Ribeiro Carrott, Suhas, Low-cost adsorbents: growing approach to wastewater treatmenta review, Crit. Rev. Environ. Sci. Technol. 39 (2009) 783–842, https://doi.org/10.1080/10643380801977610.
[31] Z. Liu, G. Chen, X. Li, X. Lu, Removal of rare earth elements by MnFe2O4 based mesoporous adsorbents: synthesis, isotherms, kinetics, thermodynamics, J. Alloys Compd. 856 (2021) 158185, https://doi.org/10.1016/j.jallcom.2020.158185.
[32] J. Pinto, R. Fernandes, D. Tavares, B. Henriques, T. Trindade, E. Pereira, Removal of rare earth elements from complex mixtures by using manganese ferrite nanoparticles: optimization through surface response methodology, J. Environ. Manag. 368 (2024), https://doi.org/10.1016/j.jenvman. 2024.122211.
[33] M.J. Atkinson, Elemental composition of commercial seasalts, J. Aquaric. Aquat. Sci. VIII (1997).
[34] E. Fabre, B. Henriques, T. Viana, J. Pinto, M. Costa, N. Ferreira, D. Tavares, C. Vale, J. Pinheiro-Torres, E. Pereira, Optimization of Nd(III) removal from water by Ulva sp. and Gracilaria sp. through Response Surface Methodology, J Environ Chem Eng 9 (2021) 105946. doi:https://doi.org/10.1016/j.jece.2021.105946.
[35] E.D. Revellame, D.L. Fortela, W. Sharp, R. Hernandez, M.E. Zappi, Adsorption kinetic modeling using pseudo-first order and pseudo-second order rate laws: a review, Clean. Eng. Technol. 1 (2020), https://doi.org/10.1016/j.clet.2020.100032.
[36] Y.S. Ho, G. McKay, A comparison of chemisorption kinetic models applied to pollutant removal on various sorbents, Process. Saf. Environ. Prot. 76 (1998) 332–340, https://doi.org/10.1205/095758298529696.
[37] Y.S. Ho, Review of second-order models for adsorption systems, J. Hazard. Mater. 136 (2006) 681–689, https://doi.org/10.1016/j.jhazmat.2005.12.043.
[38] X. Chen, Modeling of experimental adsorption isotherm data, Information (Switzerland) 6 (2015) 14–22, https://doi.org/10.3390/info6010014.
[39] R. Han, J. Zhang, W. Zou, J. Shi, H. Liu, Equilibrium biosorption isotherm for lead ion on chaff, J. Hazard. Mater. 125 (2005) 266–271, https://doi.org/10.1016/j.jhazmat.2005.05.031.
[40] J. Wang, X. Guo, Adsorption isotherm models: classification, physical meaning, application and solving method, Chemosphere 258 (2020), https://doi.org/10.1016/j.chemosphere.2020.127279.
[41] N. Ferreira, E. Fabre, B. Henriques, T. Viana, M. Costa, J. Pinto, D. Tavares, L. Carvalho, J. Pinheiro-Torres, E. Pereira, Response surface approach to optimize the removal of the critical raw material dysprosium from water through living seaweeds, J. Environ. Manag. 300 (2021), https://doi.org/10.1016/j.jenvman.2021.113697.
[42] N. Ferreira, T. Viana, B. Henriques, D.S. Tavares, J. Jacinto, J. Colónia, J. Pinto, E. Pereira, Application of response surface methodology and box–behnken design for the optimization of mercury removal by Ulva sp, J. Hazard. Mater. 445 (2023), https://doi.org/10.1016/j.jhazmat.2022.130405.
[43] Y.J. Tu, S.C. Lo, C.F. You, Selective and fast recovery of neodymium from seawater by magnetic iron oxide Fe3O4, Chem. Eng. J. 262 (2015) 966–972, https://doi.org/10.1016/j.cej.2014.10.025.
[44] W. Plazinski, W. Rudzinski, A. Plazinska, Theoretical models of sorption kinetics including a surface reaction mechanism: a review, Adv. Colloid Interf. Sci. 152 (2009) 2–13, https://doi.org/10.1016/j.cis.2009.07.009.

[45] D. Kołodyńska, J. Bąk, M. Majdańska, D. Fila, Sorption of lanthanide ions on biochar composites, J. Rare Earths 36 (2018) 1212–1220, https://doi.org/10.1016/j.jre.2018.03.027.
[46] G. de V. Brião, M.G.C. da Silva, M.G.A. Vieira, Neodymium recovery from aqueous solution through adsorption/desorption onto expanded vermiculite, Appl. Clay Sci. 198 (2020) 105825, https://doi.org/10.1016/j.clay.2020.105825.
[47] X. Liu, M. Li, S. Yang, Y. Yang, J. Nie, Y. Xue, Y. Ouyang, S. Xiao, High-performance scavenging of Nd (III) and Sm (III) from water by a copper-based metal-organic framework HKUST-1, J. Chem. Sci. 134 (68) (2022) 1–11, https://doi.org/10.1007/s12039-022-02062-0.
[48] L.C.S. Nascimento, M.L. Torem, E.C. Giese, A.G. Merma, L.C. Bertolino, N.O. A. Anjos, On the adsorption of neodymium species from aqueous solution by beneficiated palygorskite, Miner. Eng. 195 (2023) 108029, https://doi.org/10.1016/j.mineng.2023.108029.
[49] D. Kołodyńska, K. Araucz, New titanium oxide sorbent for as(V) and Cr(VI) removal as well as La(III) and Nd(III) recovery, J. Mol. Liq. 315 (2020) 113720, https://doi.org/10.1016/j.molliq.2020.113720.
[50] P. Wamea, M.L. Pitcher, J. Muthami, A. Sheikhi, Nanoengineering cellulose for the selective removal of neodymium: towards sustainable rare earth element recovery, Chem. Eng. J. 428 (2022) 131086, https://doi.org/10.1016/j.cej.2021.131086.
[51] L. Chen, X. Xiao, J. Yu, Y. Gan, Q. Chen, C. Lu, H. Dan, Y. Ding, Efficient removal of neodymium from aqueous solution by amino-functionalized SBA-15, J. Radioanal. Nucl. Chem. 331 (2022) 5789–5798, https://doi.org/10.1007/s10967-022-08635-0.
[52] B. Lapo, S. Pavón, M. Bertau, H. Demey, M. Meneses, A.M. Sastre, Neodymium recovery from the aqueous phase using a residual material from Saccharified Banana-rachis/polyethylene-glycol, Polymers (Basel) 15 (2023) 1–16, https://doi.org/10.3390/polym15071666.
[53] S.V. Durán, B. Lapo, M. Meneses, A.M. Sastre, Recovery of neodymium (III) from aqueous phase by chitosan-manganese-ferrite magnetic beads, Nanomaterials 10 (2020) 1–15, https://doi.org/10.3390/nano10061204.
[54] R. Asadi, H. Abdollahi, M. Gharabaghi, Z. Boroumand, Effective removal of Zn (II) ions from aqueous solution by the magnetic MnFe2O4 and CoFe2O4 spinel ferrite nanoparticles with focuses on synthesis, characterization, adsorption, and desorption, Adv. Powder Technol. 31 (2020) 1480–1489, https://doi.org/10.1016/j.apt.2020.01.028.
[55] V. Ghobadifar, G.B. Marandi, M. Kurdtabar, G.R. Bardajee, Removal of Pb(II) and cd(II) by MnFe2O4@SiO2@VTMS nanocomposite hydrogel from aqueous solutions, J. Polym. Environ. 31 (2023) 2686–2704, https://doi.org/10.1007/s10924-022-02670-4.
[56] F. Loulic, R. Shirazi, M. Miralinaghi, H. Panahi, E. Moniri, Highly efficient removal of toxic as(V), cd (II), and Pb(II) ions from water samples using MnFe2O4@SBA-15-(CH2)3-adenine as a recyclable bio-nanoadsorbent, Microporous Mesoporous Mater. 356 (2023) 112567, https://doi.org/10.1016/j.micromeso.2023.112567.
[57] O. Dudarko, N. Kobylinska, V. Kessler, G. Seisenbaeva, Recovery of rare earth elements from NdFeB magnet by mono- and bifunctional mesoporous silica: waste recycling strategies and perspectives, Hydrometallurgy 210 (2022), https://doi.org/10.1016/j.hydromet.2022.105855.